Theoret. Chim. Acta (Berl.) 35, 1—15 (1974)

Commentationes

Consequences of Resonance Tunnelling in Chemical Kinetics

Mohamed W. Morsy*, Ali Rabie*, Abdelazim Hilal, and Hermann Hartmann
Institut für theoretische Chemie der Universität Frankfurt am Main

Received March 1, 1974

The kinetic consequences of resonance tunnelling processes that may occur in chemical reactions are investigated in terms of a multi-centered unsymmetrical Eckart potential barrier. This potential function does not only simulate the possible existence of intermediate wells in the effective potential energy cut along the reaction path, but also is amenable to analytic solutions. The reaction rate as well as its dependence on temperature, reduced mass, Q-value, activation energy and barrier diffuseness are evaluated for successively increasing the number of barrier stages. Comparisons between results due to single and multi-humped potential energy barriers are made and discussed.

Key words: Resonance tunnelling in chemical kinetics – Eckart function – Multi-humped potential barrier

1. Introduction

Intermediate potential wells that may show up in the effective potential energy cut, along the chemical reaction path, are possibly due to the presence of hollows [1–3] in the potential energy surface or produced by the dynamic coupling between translational and vibrational motions [4–6]. Such intermediate wells are capable of trapping the activated complex into quasi-bound states, which are indicated by resonances in the tunnelling probability. This resonance contribution competes with the slowly varying direct one and consequently enhances the penetrability through the potential barrier appreciably.

Child [7] has evaluated, using the JWKB method, the penetrability factor for a general monotonic double humped barrier to provide an intermediate trap for the activated complex. Unfortunately, the involved action integrals are not amenable to be performed analytically.

Conner [8] has specialized Child's treatment for a parabolic dip joined by two inverted parabolic hills, for which analytic solutions are presumably permitted. Nevertheless, such segmental parabolic representation misdescribes the entrance and exit regions of the potential barrier. Further and more importantly, the connection formulae in the JWKB method [9] are unidirectional and consequently the validity of the method is questionable, particularly when the scattering energy is close to the top of the second hump of the potential barrier [10].

In this paper, we suggest a prescription of a multi-humped potential barrier, for which not only the correct asymptotic requirements are satisfied, but analytic

* Permanent address: Theoretical Physics Department, Atomic Energy Establishment, Cairo, Egypt.

solutions are also permitted. This can be accomplished by generalizing the double centered Eckart function [11] to any arbitrary number of centres.

The main objectives of this work are threefold: Firstly, to study the kinetic consequences of incorporating a multi-humped potential barrier in the course of calculating the chemical reaction rates. Secondly, to perform a parametric study concerning the potential parameters with the eventual purpose of probing the actual character of the effective potential energy along the reaction path. Thirdly, to search for systematic features affecting the reaction rate when different choices are made for reactants and for different temperatures.

Section 2 outlines the solution of the scattering problem corresponding to a multi-centered Eckart potential barrier, and the procedure adopted for extracting the penetrability. In Section 3, the penetrability and the chemical reaction rate are evaluated for the $H+H_2$ system. The effects of varying the temperature, reduced mass, Q-value, activation energy, barrier diffuseness and the number of barrier stages are investigated. A general discussion of the numerical results is also given. Finally in Section 4, a summary and some concluding arguments are given.

2. Theory

The key to this study is the one dimensional potential scattering equation [7, 12] which governs the translational motion:

$$\left[-\frac{\hbar^2}{2\mu(u)}\frac{\partial^2}{\partial u^2}+V(u)+\varepsilon_n(u)-E\right]F_n(u)=0 \tag{2.1}$$

in which E is the scattering energy, $V(u)$ is the potential energy barrier along the reaction coordinate u, $\varepsilon_n(u)$ is the eigenenergy belonging to the vibrational motion which is perpendicular to the reaction coordinate and $\mu(u)$ represents an effective reduced mass which may vary along the reaction coordinate.

Asymptotically, for $u\to\pm\infty$, the potential barrier, the vibrational eigenenergy and the effective mass approach constant values V^-, ε_n^-, μ^- and V^+, ε_n^+, μ^+ corresponding to reagents and products channels respectively. Consequently the solution of Eq. (2.1) can be expressed asymptotically as a linear combination of incomming and outgoing plane waves. More precisely, the asymptotic solution corresponding to the reagents channel is:

$$\lim_{u\to-\infty}F_n(u)=a_r^+\exp(ik_n^-\cdot u)+a_r^-\exp(-ik_n^-\cdot u) \tag{2.2}$$

while in the products channel there are only outgoing waves:

$$\lim_{u\to\infty}F_n(u)=a_p^+\exp(ik_n^+\cdot u) \tag{2.3}$$

where $k_n^\pm$ denotes the channel wave number:

$$k_n^\pm=\sqrt{\frac{2\mu^\pm}{\hbar^2}(E-\varepsilon_n^\pm-V^\pm)}\,. \tag{2.4}$$

At this point it is to be noted that the penetrability through the effective potential barrier:

$$\tilde{V}_n(u)=V(u)+\varepsilon_n(u) \tag{2.5}$$

is simply the ratio of the transmitted flux to the incident one:

$$P_n(E) = \frac{k_n^+ \mu^-}{k_n^- \mu^+} \left| \frac{a_h^+}{a_r^+} \right|^2 . \tag{2.6}$$

Therefrom, the chemical reaction rate can be evaluated since it is essentially the Laplace transform of the penetrability (13); namely:

$$k_n(T) = \frac{\sqrt{2\pi\hbar^2}}{(\mu^- RT)^{3/2}} \int_0^\infty dE \exp(-E/RT) P_n(E) . \tag{2.7}$$

Accordingly, the immediate task of the present work is to calculate the penetrability factor with the eventual purpose of evaluating the reaction rate constant. This task, presumably, can be achieved only after supplying not only the effective potential barrier (EPB) but also the effective reduced mass (ERM).

Let us assume, as mentioned before, that the EPB can be expressed as a linear combination of a multi-centered Eckart function of the form:

$$\tilde{V}_0(u) = \sum_{i=1}^{N} \left\{ A_i f_i(u-u_i) + B_i a_i \frac{\partial}{\partial u} f_i(u-u_i) \right\} \tag{2.8}$$

where $f_i(u-u_i)$ denotes the single Eckart function:

$$f_i(u-u_i) = \frac{1}{1+\exp(-(u-u_i)/a_i)} \tag{2.9}$$

which is nothing but a rounded unit step function centered at $u = u_i$ with the diffuseness a_i.

Presumably one can generate, by virtue of the analytic form as defined by Eq. (2.8), potential functions that do not only approach constant values in the asymptotic regions but also give rise to N humps separated by $N-1$ intermediate wells in the interaction region. The heights of the humps, E_i, as well as the depths of the wells, D_i, can be expressed in terms of the strength parameters A_i and B_i; namely

$$E_i = \frac{(A_i + B_i)^2}{4B_i} + (1-\delta_{i1}) \sum_{k=1}^{i} A_k ; \qquad i = 1, 2, \ldots, N , \tag{2.10}$$

$$D_j = \sum_{k=1}^{j} A_k ; \qquad j = 1, 2, \ldots, N-1 \tag{2.11}$$

provided that the width of each stage does not exceed the separation between the closest centres; or equivalently:

$$u_{i+1} - u_i \geqq 2\pi a_i . \tag{2.12}$$

Furthermore, let us assume that the variation of the ERM with the reaction coordinate can be also described by an Eckart step function of the form:

$$\mu(u) = \mu^- + (\mu^+ - \mu^-) f_0(u-u_0) \tag{2.13}$$

which permits smooth variation between the asymptotic reduced masses μ^- and μ^+ about $u = u_0$ along the reaction coordinate. Nevertheless, if we substitute both the EPB and ERM as given respectively by Eq. (2.8) and Eq. (2.13) into

Eq. (2.1); then after simple manipulation we can absorb the variation of the mass into the potential; namely

$$\left[-\frac{\hbar^2}{2\mu^-}\frac{\partial^2}{\partial u^2}+\sum_{i=1}^{N}\left\{\tilde{A}_i f_i(u-u_i)+\tilde{B}_i a_i\frac{\partial}{\partial u}f_i(u-u_i)\right\}\right.$$
$$\left.+(1-\mu^+/\mu^-)\,f_0(u-u_0)-E\right]F(u)=0 \tag{2.14}$$

in which $\tilde{A}_i$ and $\tilde{B}_i$ stand for the strength parameters after being appropriately scaled.

Further, if we fix u_0 to any one of the centres u_i, say u_k, then we can combine the mass term into the first member of the series representing the EPB. This implies, simply, the addition of the factor $(1-\mu^+/\mu^-)\,E$ to the strength $\tilde{A}_k$. Therefore one gets the equation

$$\left[-\frac{\hbar^2}{2\mu^-}\frac{\partial^2}{\partial u^2}+\sum_{i=1}^{N}\left\{[\tilde{A}_i+(1-\mu^+/\mu^-)\,E\delta_{ik}]\,f_i(u-u_i)\right.\right.$$
$$\left.\left.+\tilde{B}_i a_i\frac{\partial}{\partial u}f_i(u-u_i)-E\right]F(u)=0 \tag{2.15}$$

which indicates that it is possible to render the varying mass problem to a constant mass one after appropriately scaling the potential strength parameters.

Our goal now is to solve the above Eq. (2.15) with the eventual purpose of calculating the penetrability through the N-humped EPB that has been mentioned above. The natural way of approaching this problem is to divide the reaction coordinate, as depicted in Fig. 1, into N regions separated by $N-1$ boundaries, $b_1, b_2, \ldots, b_{N-1}$, that are placed at the mid-points between the centres $u_1, u_2, \ldots,$ and u_N. For each region the scattering Eq. (2.15), as we shall see latter, can be solved analytically, provided that the corresponding potential width does not exceed the separation between the closest centres. By employing the continuity condition, which requires that these regional solutions should be matched smoothly at the boundary points, it is possible to express the scattering coefficients of the last stage in terms of those belonging to the first one. The ratio of the scattering coefficients gives, essentially, the desired penetrability factor.

In order to accomplish this plan, let us consider Eq. (2.15) for which the reaction coordinate is restricted to the i^{th} region: $u\in[b_i, b_{i+1}]$; namely

$$\left[-\frac{\hbar^2}{2\mu^-}\frac{\partial^2}{\partial u^2}+\left(\tilde{A}_i+a_i\tilde{B}_i\frac{\partial}{\partial u}\right)f_i(u-u_i)-E\right]F_i(u)=0\,; \tag{2.16}$$

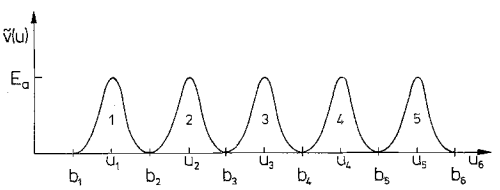

Fig. 1. Schematic multi-centered symmetrical Eckart potential function ($A_i=0$)

now by introducing the transformation [15]:

$$y_i = \frac{1}{1+\exp((u-u_i)/a_i)} \tag{2.17}$$

together with the change of the dependent variable from $F(y_i)$ to $\varphi(y_i)$ as follows

$$F(y_i) = y_i^{\nu_i}(1-y_i)^{\lambda_i}\,\varphi(y_i) \tag{2.18}$$

which after being inserted into Eq. (2.16), one finds that $\varphi(y_i)$ satisfies the hypergeometric equation [16]:

$$\left[y_i(1-y_i)\frac{\partial^2}{\partial y_i^2} + \{2\nu_i + 1 - 2(\nu_i+\lambda_i+1)\,y_i\}\frac{\partial}{\partial y_i} - (\nu_i+\lambda_i)(\nu_i+\lambda_i+1) - \frac{2\mu^- a_i^2}{\hbar^2}\tilde{B}_i\right]\varphi(y_i) = 0\,. \tag{2.19}$$

The general solution of this equation can be expressed in terms of the hypergeometric series; namely

$$\begin{aligned}\varphi(y_i) = {} & e_1 F(\tfrac{1}{2}+\nu_i+\lambda_i+\varepsilon_i,\ \tfrac{1}{2}+\nu_i+\lambda_i-\varepsilon_i;\ 2\nu_i+1;\ y_i) \\ & + e_2 y^{-2\nu_i} F(\tfrac{1}{2}-\nu_i+\lambda_i+\varepsilon_i,\ \tfrac{1}{2}-\nu_i+\lambda_i-\varepsilon_i;\ -2\nu_i+1;\ y_i)\end{aligned} \tag{2.20}$$

provided that ν_i, λ_i, and ε_i are assigned the values

$$\nu_i = i\sqrt{\frac{2\mu^- a_i^2}{\hbar^2}(E-\tilde{A}_i)} \equiv i\beta_i\,, \tag{2.21}$$

$$\lambda_i = i\sqrt{\frac{2\mu^- a_i^2}{\hbar^2}E} \equiv i\alpha_i\,, \tag{2.22}$$

$$\varepsilon_i = i\sqrt{\frac{2\mu^- a_i^2}{\hbar^2}B_i - \frac{1}{4}} \equiv i\delta_i\,. \tag{2.23}$$

Consequently, the complete solution can be written in the form

$$F(y_i) = r_i^+\,\mathscr{R}_i^+(y_i) + r_i^-\,\mathscr{R}_i^-(y_i) \tag{2.24}$$

where

$$\mathscr{R}_i^{\pm}(y_i) = (1-y_i)^{+i\alpha_i} y_i^{\mp i\beta_i} F(\tfrac{1}{2}+i(\alpha_i \mp \beta_i+\delta_i),\ \tfrac{1}{2}+i(\alpha_i\mp\beta_i-\delta_i);\ 1\mp 2i\beta_i;\ y_i) \tag{2.25}$$

in which the hypergeometric series remain convergent as long as y_i is small or u is restricted to be $u \geqq u_i$. Nevertheless, the above solution can be extended to the region $u \leqq u_i$, by continuing the hypergeometric series analytically [16]. This enables us to cast the complete solution as given by Eq. (2.24) into an alternative form which is convergent in the region $u \leqq u_i$; namely:

$$F(y_i) = l_i^+\,\mathscr{L}_i^+(y_i) + l_i^-\,\mathscr{L}_i^-(y_i) \tag{2.26}$$

where

$$\begin{aligned}&\mathscr{L}_i^{\pm}(y_i) \\ &= (1-y_i)^{\pm i\alpha_i} y_i^{-i\beta_i} F(\tfrac{1}{2}+i(\pm\alpha_i-\beta_i+\delta_i),\ \tfrac{1}{2}+i(\pm\alpha_i-\beta_i-\delta_i);\ 1\pm 2i\alpha_i;\ 1-y_i)\end{aligned} \tag{2.27}$$

and

$$l_i^{\pm} = r_i^{+} c_i^{\pm} + r_i^{-} d_2^{\pm} \tag{2.28}$$

in which

$$c_i^{\pm} = \frac{\Gamma(\mp 2i\alpha_i)\,\Gamma(1-2i\beta_i)}{\Gamma(\frac{1}{2}+i(\mp\alpha_i-\beta_i+\delta_i))\,\Gamma(\frac{1}{2}+i(\mp\alpha_i-\beta_i-\delta_i))} \tag{2.29}$$

and

$$d_i^{\pm} = \frac{\Gamma(\mp 2i\alpha_i)\,\Gamma(1+2i\beta_i)}{\Gamma(\frac{1}{2}+i(\mp\alpha_i+\beta_i-\delta_i))\,\Gamma(\frac{1}{2}+i(\mp\alpha_i+\beta_i-\delta_i))}\,. \tag{2.30}$$

Before proceeding to calculate the penetrability, we first need the asymptotic behaviour of $\mathscr{R}_i(y_i)$ and $\mathscr{L}_i(y_i)$ at infinitely positive and negative values of u respectively. This can be easily accomplished in view of the fact that the hypergeometric series involved in Eq. (2.25) and Eq. (2.27) become unity as the arguments y_i and $1-y_i$ approach zero. Accordingly, we get

$$\lim_{u\to+\infty} \mathscr{R}_i^{\pm}(y_i) = \exp(\pm i\beta_i a_i u) \tag{2.31}$$

and

$$\lim_{u\to-\infty} \mathscr{L}_i^{\pm}(y_i) = \exp(\pm i\alpha_i a_i u) \tag{2.32}$$

which indicate that the correct asymptotic requirements are inherited in each stage.

Our aim now is to express the amplitude coefficients belonging to the first potential hump in terms of those belonging to the last one in order to extract the penetrability factor as given by Eq. (2.26). This can be accomplished by employing the continuity condition which requires that the regional solutions should be matched successively at the connecting boundary points. These requirements provide $2\cdot(N-1)$ linear equations connecting the amplitude coefficients belonging to adjacent regions i and $i+1$ of the form:

$$r_i^{+}\mathscr{R}_i^{+}(b_i) + r_i^{-}\mathscr{R}_i^{-}(b_i) = l_{i+1}^{+}\mathscr{L}_{i+1}^{+}(b_i) + l_{i+1}^{-}\mathscr{L}_{i+1}^{-}(b_i)\,, \tag{2.33}$$

$$r_i^{+}\dot{\mathscr{R}}_i^{+}(b_i) + r_i^{-}\dot{\mathscr{R}}_i(b_i) = l_{i+1}^{+}\dot{\mathscr{L}}_{i+1}^{+}(b_i) + l_{i+1}^{-}\dot{\mathscr{L}}_{i+1}^{-}(b_i)\,, \tag{2.34}$$

where i is allowed to take the values 1, 2, ... up to $N-1$, and the dot refers to the differentiation with respect to u. These derivatives explicitely read:

$$\begin{aligned}\mathscr{D}_u\mathscr{R}_i^{\pm}(y_i) = a_i^{-1} y_i^{\mp i\beta_i}(1-y_i)^{i\alpha_i+1}\{&[\mp i\beta_i + i\alpha_i y_i/(1-y_i)]\\ &\cdot F(\tfrac{1}{2}+i(\alpha_i\mp\beta_i+\delta_i), \tfrac{1}{2}+i(\alpha_i\mp\beta_i-\delta_i); 1\mp 2i\beta_i; y_i)\\ &+ \frac{(\frac{1}{2}+i(\alpha_i\mp\beta_i+\delta_i))\,(\frac{1}{2}+i(\alpha_i\mp\beta_i-\delta_i))}{1\mp 2i\beta_i} y_i\\ &\cdot F(\tfrac{3}{2}+i(\alpha_i\mp\beta_i+\delta_i), \tfrac{3}{2}+i(\alpha_i\mp\beta_i-\delta_i); 2(1\mp i\beta_i); y_i)\}\end{aligned} \tag{2.35}$$

and

$$\begin{aligned}\mathscr{D}_u\mathscr{L}_i^{\pm}(y_i) = a_i^{-1} y_i^{-i\beta_i}(1-y_i)^{\pm i\alpha_i+1}\{&[-i\beta_i \pm i\alpha_i y_i/(1-y_i)]\\ &\cdot F(\tfrac{1}{2}+i(\pm\alpha_i-\beta_i+\delta_i), \tfrac{1}{2}+i(\pm\alpha_i-\beta_i-\delta_i); 1\pm 2i\alpha_i; 1-y_i)\\ &+ \frac{(\frac{1}{2}+i(\pm\alpha_i-\beta_i+\delta_i))\,(\frac{1}{2}+i(\pm\alpha_i-\beta_i-\delta_i))}{1\mp 2i\beta_i} y_i\\ &\cdot F(\tfrac{3}{2}+i(\pm\alpha_i-\beta_i+\delta_i), \tfrac{3}{2}+i(\pm\alpha_i-\beta_i-\delta_i); 2(1\pm i\alpha_i); 1-y_i)\}\,.\end{aligned} \tag{2.36}$$

Furthermore, the amplitude coefficients l_{i+1}^{+} and l_{i+1}^{-} are in fact related to r_{i+1}^{+} and r_{i+1}^{-} by virtue of Eq. (2.28). Therefore one can eliminate l_{i+1}^{+} and l_{i+1}^{-} and obtain recurrence relation which can be expressed in the matrix form:

$$\begin{pmatrix} r_i^{+} \\ r_i^{-} \end{pmatrix} = \begin{pmatrix} \mathscr{R}_i^{+}(b_i) & \mathscr{R}_i^{-}(b_i) \\ \dot{\mathscr{R}}_i^{+}(b_i) & \dot{\mathscr{R}}_i^{-}(b_i) \end{pmatrix}^{-1} \begin{pmatrix} \mathscr{L}_{i+1}^{+}(b_i) & \mathscr{L}_{i+1}^{-}(b_i) \\ \dot{\mathscr{L}}_{i+1}^{+}(b_i) & \dot{\mathscr{L}}_{i+1}^{-}(b_i) \end{pmatrix} \begin{pmatrix} c_{i+1}^{+} & d_{i+1}^{+} \\ c_{i+1}^{-} & d_{i+1}^{-} \end{pmatrix} \begin{pmatrix} r_{i+1}^{+} \\ r_{i+1}^{-} \end{pmatrix}. \tag{2.37}$$

Therefrom one obtains for the penetrability

$$P(E) = \frac{\alpha_N}{\alpha_1} \frac{\mu^{-}}{\mu^{+}} \left| \frac{r_N^{+}}{r_1^{+}} \right|^2 \tag{2.38}$$

from iterating Eq. (2.35) $(N-1)$ times after being subjected to the outgoing boundary condition as given by Eq. (2.24).

At this point it is of interest to specialize the generalized treatment mentioned above to the simple case where one potential hump is allowed in the EPB. This can be immediately accomplished by restricting the index N to be one and as a consequence Eq. (2.15) reduces to

$$\left[-\frac{\hbar^2}{2\mu^{-}} \frac{\partial^2}{\partial u^2} + \left([\tilde{A}_1 + (1-\mu^{+}/\mu^{-})\, E] + a_1 \tilde{B}_1 \frac{\partial}{\partial u} \right) f_1(u-u_1) - E \right] F_1(u) = 0 \tag{2.39}$$

which in view of Eq. (2.24) and Eq. (2.26) together with the outgoing boundary condition as given by Eq. (2.3) which possesses the solutions:

$$F(u) = r_1^{+} \mathscr{R}_1^{+}(y_1) \tag{2.40a}$$

and

$$F(u) = r_1^{+} c_1^{+} \mathscr{L}_1^{+}(y_1) + r_1^{+} c_{1,}^{-} \mathscr{L}_1^{-}(y_1) \tag{2.40b}$$

which are not only continuous at $u = u_1$ but also satisfy the correct asymptotic requirements.

The penetrability can be calculated either from the ratio of the transmitted flux to the incident one or from the reflection coefficient

$$\mathbb{R} = \left| \frac{c_1^{-}}{c_1^{+}} \right|^2 \tag{2.41}$$

after exploiting the fact that the total flux is conserved

$$P = 1 - \mathbb{R}. \tag{2.42}$$

In this case the latter approach is simpler, and consequently after employing Eq. (2.29), the reflection coefficient explicitly reads:

$$\mathbb{R} = \left| \frac{\Gamma(\frac{1}{2} + i(\delta_1 - \beta_1 - \alpha_1))\, \Gamma(\frac{1}{2} + i(-\delta_1 - \beta_1 - \alpha_1))}{\Gamma(\frac{1}{2} + i(\delta_1 - \beta_1 + \alpha_1))\, \Gamma(\frac{1}{2} + i(-\delta_1 - \beta_1 + \alpha_1))} \right|^2 \tag{2.43}$$

which by virtue of the relation

$$\Gamma\left(\frac{1}{2} + i\vartheta\right) = \sqrt{\frac{\pi}{\cosh \pi\vartheta}} \tag{2.44}$$

becomes

$$P = 1 - \frac{\cosh[\pi(\delta_1 - \beta_1 + \alpha_1)] \cosh[\pi(-\delta_1 - \beta_1 + \alpha_1)]}{\cosh[\pi(\delta_1 + \beta_1 - \alpha_1)] \cosh[\pi(\delta_1 + \beta_1 + \alpha_1)]} \tag{2.45}$$

from which one acts, for the penetrability, the closed form expression [14]

$$P = 1 - \frac{\cosh[2\pi(\alpha_1 - \beta_1)] + \cosh[2\pi\delta_1]}{\cosh[2\pi(\alpha_1 + \beta_1)] + \cosh[2\pi\delta_1]}. \tag{2.46}$$

However it is to be noted that the effect of allowing the reduced mass to vary along the reaction coordinate is included in the scaled strength parameters $\tilde{A}_1$ and $\tilde{B}_1$. Nevertheless, it can be easily shown that they can be expressed explicitely as:

$$\tilde{A}_1 = A_1 \mu^+/\mu^- \tag{2.47}$$

and

$$\tilde{B}_1 = B_1(1 + \mu^+/\mu^-)/2 \tag{2.48}$$

by virtue of which α_i, β_i and δ_i become:

$$\alpha_1 = \frac{a_i}{\hbar}\sqrt{2\mu^- E} \tag{2.49}$$

$$\beta_1 = \frac{a_i}{\hbar}\sqrt{2\mu^-(E - A_1)} \tag{2.50}$$

and

$$\delta_1 = \frac{a_i}{\hbar}\sqrt{B_1(\mu^+ + \mu^-) - \frac{\hbar^2}{4a_1^2}} \tag{2.51}$$

which are reducible to the conventional expressions for the case of fixing the reduced mass ($\mu^+ = \mu^-$).

3. Results and Discussion

In this section we report the actual computations of the penetrability factor and its Laplace transform on the basis of the procedure that has been outlined in the previous section. This task is made for the purpose of studying the kinetic consequences of incorporating a multi-humped Eckart potential barrier along the reaction coordinate.

The plan of the computational work can be divided into three consecutive stages: First, we develope the necessary algorithm to generate the hypergeometric and Gamma functions that are involved in the penetrability factor as well as the numerical integration subroutine which is required for computerizing the chemical reaction rate. Second, we determine all the physical parameters occuring into the scattering problem from the relevant data. Third, we perform the appropriate repetitions by which it is possible to study the effect of varying, temperature, reduced mass, Q-value, activation energy, barrier diffuseness and the number of barrier stages.

The atomic mass unit (a.m.u.), the kilo calorie (kcal) and the Angstroem (Å) have been chosen to be the units of the mass, energy and length respectively.

The hypergeometric functions, which occur in the scattering solution, are generated using the series representation:

$$F(a, b; c; y) = \frac{\Gamma(c)}{\Gamma(a)\,\Gamma(b)} \sum_{n=0}^{\infty} \frac{\Gamma(a+n)\,\Gamma(b+n)}{\Gamma(c+n)\,\Gamma(n+1)}\, y^n \tag{3.1}$$

which is absolutely convergent when $|u|<1$ and c is restricted not to be negative integer [16]. In fact a, b, and c are allowed to be complex.

For the Gamma functions of complex argument such as

$$\Gamma(x+iy)=|\Gamma(x+iy)|\exp(i\arg\Gamma(x+iy)) \tag{3.2}$$

which are present in the scattering amplitudes, we employed the expressions [17]:

$$|\Gamma(x+iy)|=\Gamma(x)\prod_{n=0}^{\infty}\left[1+\frac{y^2}{(x+n)^2}\right]^{-1/2} \tag{3.3}$$

and

$$\arg\Gamma(x+iy)=y\psi(x)+\sum_{n=0}^{\infty}\left(\frac{y}{x+n}-\arctan\frac{y}{x+n}\right) \tag{3.4}$$

where $\psi(x)$ denotes the logarithmic derivative

$$\psi(x)=\Gamma'(x)/\Gamma(x)\,. \tag{3.5}$$

Nevertheless, we are specially interested in the case where x is either $1/2$ or 1. For such cases Eq. (3.3) and Eq. (3.5) become simply

$$\left|\Gamma\left(\frac{1}{2}+iy\right)\right|=\sqrt{\frac{\pi}{\cosh\pi y}}\,, \tag{3.6a}$$

$$|\Gamma(1+iy)|=\sqrt{\frac{\pi}{y\sinh\pi y}}\,, \tag{3.6b}$$

$$\psi(\tfrac{1}{2})=-\gamma-2\ln 2\,, \tag{3.7a}$$

$$\psi(1)=-\gamma=-0.5772156649\,. \tag{3.7b}$$

The extended Simpson's rule [17] is applied for performing the numerical integrations involved in the evaluation of the chemical reaction rate after properly adjusting the integration interval to match the resonance structure which may show up in the integrand.

As a test example, the reactions:

$$\mathrm{H}+\mathrm{H_2}\rightarrow\mathrm{H_2}+\mathrm{H}\,, \tag{3.8}$$

$$\mathrm{D}+\mathrm{D_2}\rightarrow\mathrm{D_2}+\mathrm{D}\,, \tag{3.9}$$

$$\mathrm{D}+\mathrm{H_2}\rightarrow\mathrm{DH}+\mathrm{H}\,, \tag{3.10}$$

$$\mathrm{H}+\mathrm{HD}\rightarrow\mathrm{H_2}+\mathrm{D}\,, \tag{3.11}$$

$$\mathrm{H}+\mathrm{D_2}\rightarrow\mathrm{HD}+\mathrm{D}\,, \tag{3.12}$$

$$\mathrm{D}+\mathrm{DH}\rightarrow\mathrm{D_2}+\mathrm{H}\,, \tag{3.13}$$

$$\mathrm{H}+\mathrm{DH}\rightarrow\mathrm{HD}+\mathrm{H}\,, \tag{3.14}$$

$$\mathrm{D}+\mathrm{HD}\rightarrow\mathrm{DH}+\mathrm{D} \tag{3.15}$$

have been considered not only for the significance of the (H, H_2) system, but also for the availability of the potential energy data [6, 18].

Table 1. Characteristics of the potential energy surfaces for the reactions indicated above

No.	Reaction	$V(u^*)$	$\varepsilon_0(u^*)$	$\varepsilon_0(-\infty)$	E_a	B	μ
		kcal/mole					a.m.u.
1	$H+H_2 \rightarrow H_2+H$	9.130	3.122	6.201	6.051	24.204	0.672
2	$D+D_2 \rightarrow D_2+D$	9.130	2.208	4.385	6.953	27.912	1.344
3	$D+H_2 \rightarrow DH+H$	9.130	2.681	6.201	5.610	22.440	1.008
4	$H+HD \rightarrow H_2+D$	9.130	2.591	5.370	6.441	25.764	0.756
5	$H+D_2 \rightarrow HD+D$	9.130	2.675	4.385	7.420	29.680	0.806
6	$D+DH \rightarrow D_2+H$	9.130	3.675	5.370	6.435	25.740	1.209
7	$H+DH \rightarrow HD+H$	9.130	3.122	5.370	6.992	27.528	0.756
8	$H+HD \rightarrow HD+H$	9.130	2.208	5.370	5.969	23.972	1.209

The values of the static potential energy barrier $V(u^*)$ at the saddle point u^*, together with the zero-point vibrational energies $\varepsilon_0(u^*)$ and $\varepsilon_0(-\infty)$, which correspond to the reactions (3.8–3.15), are listed in Table 1. The activation energy E_0 measured from the zero-point vibrational energy:

$$E_a = V(u^*) + \varepsilon_0(u^*) - \varepsilon_0(-\infty) \tag{3.16}$$

is also listed in the fifth column of Table 1.

By virtue of Eq. (2.10) and the activation energy the value of the strength parameter B, that is responsible for symmetrical shapes, can be easely shown to be

$$B = E_a \tag{3.17}$$

in view of the fact that the Q-values of the reactions considered above are zero ($A=0$). Figures 2–3 show respectively the penetrability as a function of the scattering energy and the Arrhenius plot of the chemical reaction rate that correspond to the reactions listed above for a single humped EPB with a diffuseness of $a=0.2$. It is to be noted that the penetrabilities show slowly varying step functions and the corresponding Arrhenius plots are nonlinear. Naturally, this is expected from single humped barriers. Further, it is interesting that the tunnelling probability is inversely proportional to both of the barrier height and the reduced mass.

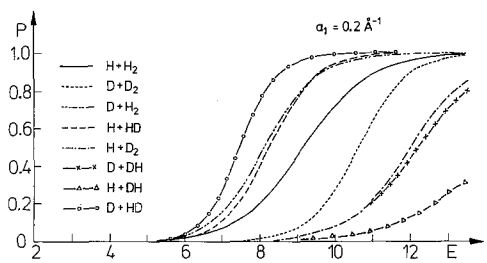

Fig. 2. Scattering energy dependence of the penetrability through single humped potential barriers that correspond to the reactions indicated. The diffuseness parameter a is taken to be ·2 for all the reactions considered

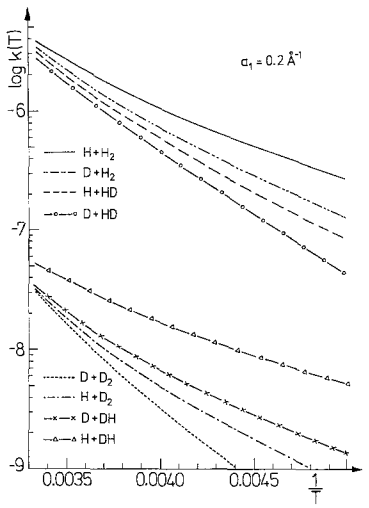

Fig. 3. Arrhenius plots of $\log k$ against $1/T$ for the reactions studied here. These plots correspond to the penetrabilities that are shown in Fig. 2

The effect of varying the diffuseness and the number of potential humps are only investigated for the first reaction $H + H_2 \rightarrow H_2 + H$. The corresponding results are depicted in Figs. 4–13 which represent the penetrability and the Arrhenius plots that correspond to one, two, three, four, and five identical potential stages and for several values of the diffuseness parameter as listed in Table 2. The separation between the potential stages is taken to be

$$u_{i+1} - u_i = 10\, a_i \tag{3.18}$$

in order to minimize the overlap between adjacent stages. The diffuseness parameters are chosen such that

$$a_i = a_1/i \qquad i = 2, 3, 4, \text{ and } 5 \tag{3.19}$$

which ensures the same total width of the EPB whatever the number of potential stages are.

Table 2. Scheme of the diffuseness and seperation parameters as function of the single stage diffuseness parameter a and the number of potential stages, *i*. a is varied from 0.5 down to 0.2 in steps of 0.1 while the number *i* of stages is varied from two up to five

N	1	2		3			4				5				
a_N	0.5	0.25	0.25	−0.170	0.170	0.170	0.125	0.125	0.125	0.125	0.10	0.10	0.10	0.10	0.10
u_N	0.0	−1.25	1.25	−0.170	0.000	1.700	−1.875	−0.625	0.625	1.875	−2.00	−1.00	0.00	1.00	2.00
a_N	0.4	0.20	0.20	0.130	0.130	0.130	0.100	0.100	0.100	0.100	0.08	0.08	0.08	0.08	0.08
u_N	0.0	−1.00	1.00	−1.300	0.000	1.300	−1.500	−0.500	0.500	1.500	−1.60	−0.80	0.00	0.80	1.60
a_N	0.3	0.15	0.15	0.100	0.100	0.100	0.075	0.075	0.075	0.075	0.06	0.06	0.06	0.06	0.06
u_N	0.0	−0.75	0.75	−1.000	0.000	1.000	1.125	−0.375	0.375	1.125	−1.20	−0.60	0.00	0.60	1.20
a_N	0.2	0.10	0.10	0.067	0.067	0.067	0.050	0.050	0.050	0.050	0.04	0.04	0.04	0.04	0.04
u_N	0.0	−0.50	0.50	−0.675	0.000	0.678	−0.750	−0.250	0.250	0.750	−0.08	−0.40	0.00	0.40	0.80

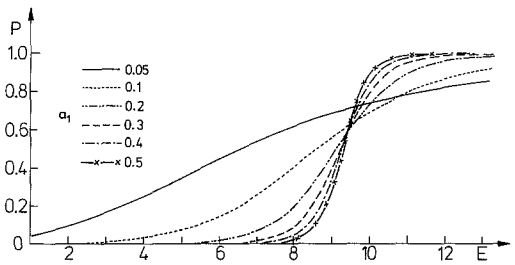

Fig. 4. The effect of varying the diffuseness parameter upon the penetrability through single stage potential barriers. The values of the diffuseness parameters employed are indicated

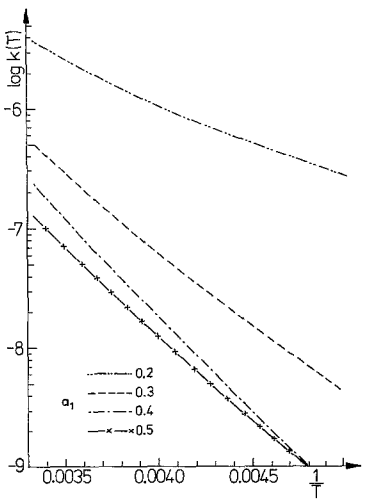

Fig. 5. The effect of varying the diffuseness parameter on the Arrhenius plots of $\log_{10} k$ against $1/T$. These plots correspond to the penetrabilities that are shown in Fig. 4

The variation of the diffuseness parameter a_1 concerning the single stage EPB affects not only the slope of the penetrability step function, but also its threshold. This is clearly shown in Fig. 4. In fact, both of the slope and the threshold are increasing functions of the diffuseness. Accordingly, the chemical reaction rate becomes enhanced as the diffuseness is decreased as shown in Fig. 5. The main reason behind this is lowering the threshold which is further amplified by the exponential kernel that occurs in the Laplace transform.

The most distinctive feature that characterizes Figs. 6, 8, 10, 12 is the appearance of resonances in the penetrability when more than one potential stage are allowed in the EPB. These resonances indicate the quasi-bound states that are set up in the intermediate wells, and their widths are inversely proportional to the half life times of the activated complex that is trapped in such states. However, it is rather difficult to draw general rules that can describe resonance tunnelling phenomena from the penetrability curves. Nevertheless it is fairly clear, as can be seen from Figs. 7, 9, 11, and 13, that the chemical reaction rate gets enhanced as the number of potential stages in the EPB increases apart from some exceptions

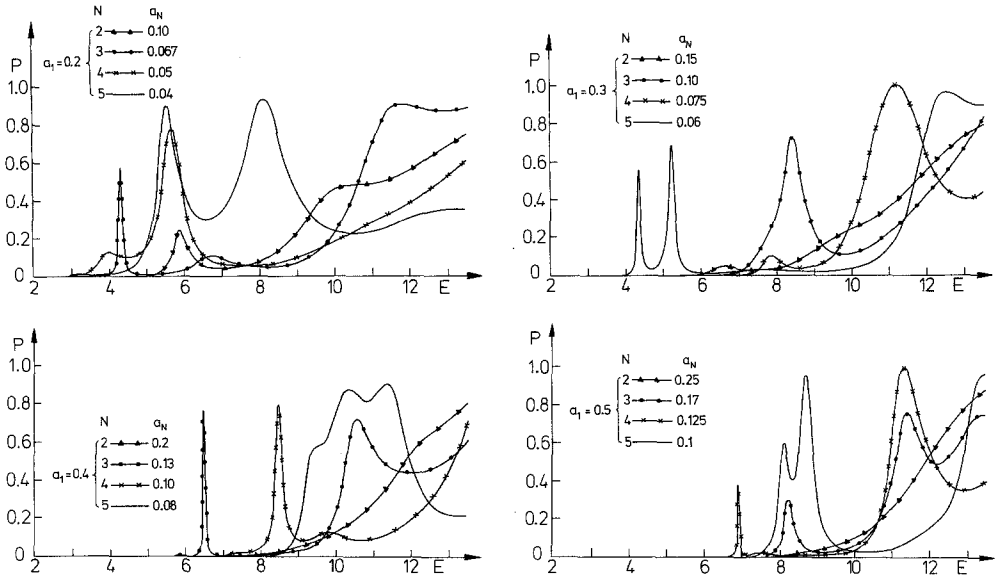

Fig. 6, 8, 10, 12. The effect of varying the number of potential stages on the penetrability through potential barriers of identical stages. The value of the diffuseness parameters employed in each number of stages are indicated. These values can be obtained by dividing the stage diffuseness parameter, a, by the number of stages

which occur for small values of the diffuseness parameter. The reason behind this lies in the fact that as we increase the number of potential stage resonance tunnelling contribution by turn increases, particularly, in the lower energies which affect appreciably the chemical reaction rate.

Furthermore, it is to be added that as we increase the depth of the intermediate wells then the density of the quasi-bound states increases and consequently the resonance tunnelling contribution increases too.

4. Summary and Conclusions

In this paper, we have developed a generalized treatment of tunnelling phenomena in chemical reactions, on the basis of adiabatic approximation and in terms of a multi-centered Eckart potential barrier. Evidently, such treatment provides not only unified description of both direct as well as resonance tunnelling, but also enables us to probe the actual character of the potential energy barrier.

The effect of including intermediate wells in the effective potential barrier has been thoroughly investigated. It is to be noted that tunnelling probability increases with increasing the number of intermediate wells. On the other hand the tunnelling probability decreases with increasing the value of the diffuseness parameter.

In conclusion, we wish to draw the attention to some advantages and drawbacks which seem to be inherent in the treatment we presented. As an advantage, the multi-centered Eckart potential is not only flexible, but also permits analytic

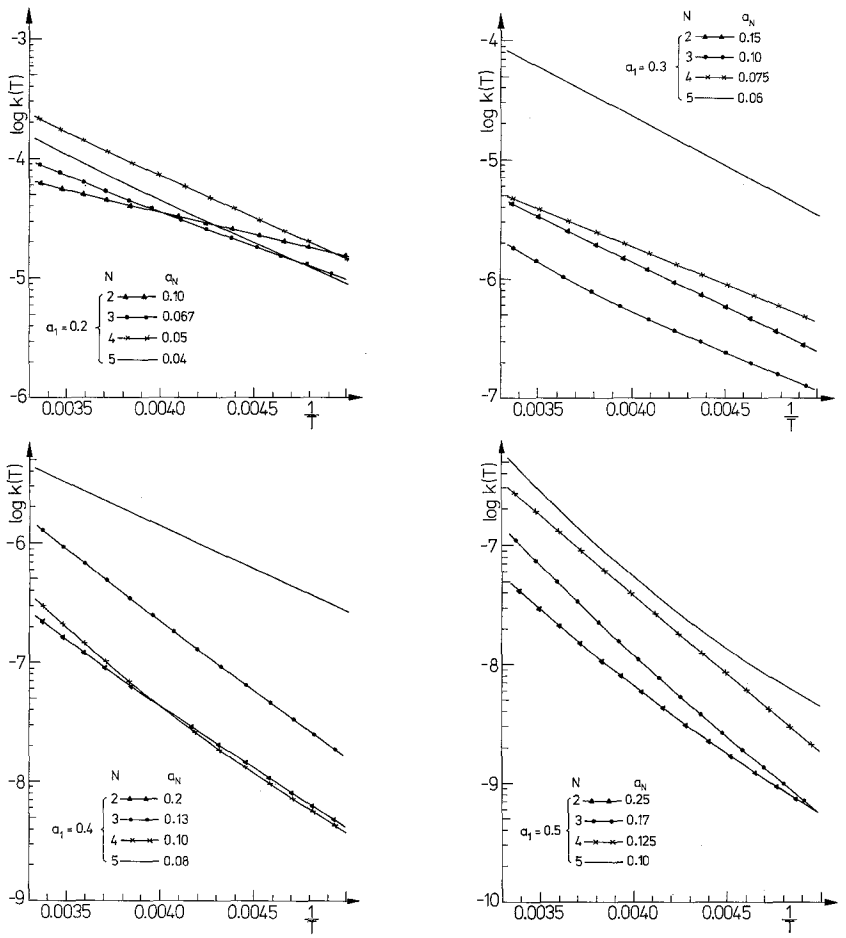

Fig. 7, 9, 11, 13. The effect of varying the number of potential stages on the Arrhenius plots of $\log k$ against $1/T$. These plots correspond to penetrabilities that are shown in the preceding figure

scattering solution. In addition the correct asymptotic shape requirements are insured. Further and more importantly, the variation of the reduced mass along the reaction coordinate can be included in the scaling of the potential parameters.

However, the possibility of the procedure hinges upon the validity of the adiabatic approximation [7]. This implies that our treatment, if applicable at all, is restricted to cases for which the nonadiabatic effects can be neglected. There is yet another difficulty inherent in our approach. If we think of our extended tunnelling treatment as a decoupled single channel scattering problem, then the effect of the other competing channels should be manifested, at least, by allowing the effective potential barrier to be complex. However, such a study is in progress [12].

Acknowledgements. This work has been supported by the Deutsche Forschungsgemeinschaft and the Akademie der Wissenschaften und Literatur zu Mainz. The numerical calculations have been performed on the UNIVAC 1108 of the Zentrales Recheninstitut der Universität Frankfurt am Main.

References

1. Roach, A.C., Child, M.S.: Mol. Phys. **14**, 1 (1965)
2. Csizmadia, I.G., Polanyi, I.C., Roach, A.C., Wong, W.H.: Can. J. Chem. **47**, 4079 (1969)
3. Polanyi, J.C.: Accounts Chem. Res. **5**, 161 (1972)
4. Levine, R.D., Wu, S.-F.: Chem. Phys. Letters **15**, 557 (1971)
5. Wu, S.-F., Levine, R.D.: Mol. Phys. **22**, 881 (1971)
6. Wu, S.-F., Johnson, B.R., Levine, R.D.: Mol. Phys. **25**, 609 (1973)
7. Child, M.S.: Mol. Phys. **12**, 401 (1968)
8. Conner, J.N.L.: Mol. Phys. **15**, 37 (1968)
9. Fröman, N., Fröman, P.O.: JWKB Approximation, Amsterdam: North Holland 1955
10. Leboeuf, J.N., Sharma, R.C.: Can. J. Phys. **51**, 446 (1973)
11. Morsy, M.W.: Theoret. Chim. Acta (Berl.), To be published
12. Morsy, M.W., Hilal, A., Rabie, A., Hartmann, H.: Mol. Phys., to be published
13. Smith, F.T.: J. Chem. Phys. **36**, 248 (1962)
14. Eckart, C.: Phys. Rev. **35**, 1303 (1930)
15. Flügge, S.: Practical quantum mechanics I, p. 86. Berlin-Heidelberg-New York: Springer 1971
16. Erdelyi, A.: Higher Transendental Functions I, p. 56. New York: McGraw Hill 1953
17. Abramowitz, M., Stegun, I.A.: Handbook of mathematical functions. New York: Dover Publications 1965
18. Porter, R.N., Karplus, M.: J. Chem. Phys. **40**, 1105 (1964)

Prof. Dr. M. W. Morsy
Institut für theoretische Chemie
der Universität Frankfurt
D-6000 Frankfurt am Main
Robert-Mayer-Straße 11
Federal Republic of Germany